The nature of interfaces and charge trapping sites in photocatalytic mixed-phase TiO_2 from first principles modeling

Juan C. Garcia, Michael Nolan, and N. Aaron Deskins

Citation: The Journal of Chemical Physics **142**, 024708 (2015);
View online: https://doi.org/10.1063/1.4905122
View Table of Contents: http://aip.scitation.org/toc/jcp/142/2
Published by the American Institute of Physics

The nature of interfaces and charge trapping sites in photocatalytic mixed-phase TiO_2 from first principles modeling

Juan C. Garcia,[1] Michael Nolan,[2] and N. Aaron Deskins[1,a)]
[1]*Department of Chemical Engineering, Worcester Polytechnic Institute, 100 Institute Road, Worcester, Massachusetts 01609, USA*
[2]*Tyndall National Institute, University College Cork, Lee Maltings, Dyke Parade, Cork, Ireland*

(Received 19 September 2014; accepted 15 December 2014; published online 12 January 2015)

Mixed phase rutile/anatase catalysts show increased reactivity compared with the pure phases alone. However, the mechanism causing this effect is not fully understood. The electronic properties of the interface and the relative energy of the electron in each phase play a key role in lowering the rate of recombination of electron hole pairs. Using density functional theory and the +U correction, we calculated the bands offsets between the phases taking into account the effect of the interface. Our model included several thousands atoms, and thus is a good representation of an interface between actual nanoparticles. We found rutile to have both higher conduction and valence band offsets than rutile, leading to an accumulation of electrons in the anatase phase accompanied by hole accumulation in the rutile phase. We also probed the electronic structure of our heterostructure and found a gap state caused by electrons localized in undercoordinated Ti atoms which were present within the interfacial region. Interfaces between bulk materials and between exposed surfaces both showed electron trapping at undercoordinated sites. These undercoordinated (typically four) atoms present localized electrons that could enable reduction reactions in the interfacial region, and could explain the increased reactivity of mixed-phase TiO_2 photocatalyst materials. © *2015 AIP Publishing LLC.* [http://dx.doi.org/10.1063/1.4905122]

I. INTRODUCTION

The physical and chemical properties of TiO_2 have been extensively studied, due to its wide range of applications. It is used as a photocatalyst, a gas sensor, in medical implantations, in hydrophobic glass, and corrosion protection.[1] It has become the prototypical material for photocatalytic processes, and its rutile (110) surface is a prototype for surface science studies of metal oxides. TiO_2 photocatalysts consisting of two intimately connected phases have been demonstrated to show increased catalytic activity over single-phase catalysts (whether they be rutile or anatase), in some cases, with even up to ten times more activity.[2–7] The reason for the increased reactivity is, however, still under debate (see, for example, a recent review article[8]), but could involve several factors, including bulk charge separation, interfacial charge transfer effects, or special interfacial reaction sites, such as low coordinated Ti. While EPR studies of rutile-anatase systems have indicated that low coordinated Ti sites are likely to trap electrons,[9] the details of the interface are extremely difficult to obtain from experiments and hence, first principles simulations can be invaluable in this regard. In this article, we modeled using density functional theory (DFT) the interface between rutile and anatase phases of TiO_2 in order to further explain the mechanism of the increased photo-reactivity of these mixed-phase catalysts.

The process of heterogeneous photocatalysis over semiconductors starts with the generation of electron-hole pairs due to photoexcitation of an electron to the conduction band (CB), creating a hole in the valence band (VB). These electrons and holes may then diffuse to the surface, and transfer to adsorbed species initiating surface reduction/oxidation reactions.[10] Alternatively, the electron-hole pair may recombine with a concomitant release of energy. This competitive recombination pathway is undesired since it lowers the concentration of active electrons and holes. Much research on TiO_2 photocatalysis has focused on either increasing the production of more electron-hole pairs through for instance band-gap engineering,[11] or attempting to reduce the recombination rates.[12–14]

Mixed phase photocatalysts appear to be a superior material over single phase TiO_2 and there have been several attempts to explain the increased activity of the mixed phase catalysts.[8] The most accepted hypothesis is that presence of the two phases lowers the electron-hole recombination rate (through preferential charge migration to the various phases, or increased charge separation), which increases the number of surface electrons/holes, and therefore the surface reactivity.[15–17] The preferred phase of the electrons (or holes) is determined by the relative energy of the two phases' conduction bands (or valence bands). The alignments of the CB minimum and VB maximum of rutile and anatase have been under intense debate, with different studies indicating contradictory results.[15,16,18] Most recent results suggest that the rutile VB and CB lie higher than the anatase VB and CB.[19,20] Therefore, this is consistent with experiments suggesting that photo-generated electrons may migrate from rutile to anatase, due in part to trapping sites in the anatase

a)Author to whom correspondence should be addressed. Electronic mail: nadeskins@wpi.edu

lattice.[4] A recent combined experimental and theoretical work[21] also confirmed the higher energy level of the rutile phase conduction and valence bands. Strong interfacial regions between the phases have been suggested to facilitate charge transfer.[22–24] Other work attributes special four-coordinated Ti interfacial sites as contributing to the increased photo reactivity.[9,15,25,26]

Band offsets at semiconductor heterojunctions are fundamental parameters which govern the transport properties of electrons, and the differences in energy of the bands determine the direction and magnitude of the electrical current.[27] The estimation of the band offsets for semiconductor interfaces is crucial to understand the behavior of a metal oxide mixed phase catalysts. In order to determine offsets using electronic structure techniques, it is typically necessary to simulate an interface between the two materials.[28] However, in practice, this is rarely done, in part due to the difficulty and complexity of modeling an interface between two different crystal phases (in contrast to, e.g., interfaces in III-V layered materials with the same phase[29–31]). There have been some attempts to determine offsets, primarily using the bulk energy levels (suitably referenced) of the different constituents.[19,32] However, the detailed atomic and electronic properties at the interface are known to influence the band offsets[33] and key photocatalytic properties. A recent paper predicted the band offsets of rutile and anatase modeling an interface with the QM/MM (quantum mechanics/molecular mechanics) approach, but did not give details on the interfacial region.[20] The geometry of the interface could induce the formation of trapping sites and dipoles, which could affect the band structure. While these are difficult to probe experimentally and are not treated in simple bulk band alignment studies, the power of modern electronic structure calculations is that one can determine band offsets between two materials in an explicit interface model, and quantify the nature of the interfacial region.

We present electronic structure calculations (DFT) of realistic rutile-anatase interfaces. We calculated the relative stability of electrons/holes in each phase, taking into account the presence of the interface. The electronic structure of the interface is also studied and the nature of under-coordinated Ti sites is shown. The bulk of the analysis is performed on interfaces formed by bringing two surfaces together so that no exposed surface regions exist (bulk interface), but an interfacial structure with exposed surfaces is also used. Our analysis of the interfacial region for all interfaces provides key information on the interface and its role during photocatalysis. We acknowledge that defects (such as O vacancies or Ti interstitials) may affect the electronic properties of mixed-phase interfaces, and future work is needed to refine the structure/nature of the interfaces. Nonetheless, our work is a significant advancement in modeling and understanding mixed-phase TiO_2 materials.

II. METHODOLOGY

In this paper, we modeled interfaces formed by bringing together surfaces of rutile and anatase TiO_2. Interfacial simulations involving periodic boundary conditions require finding common lattice vectors between the two materials in the two directions parallel to the surfaces being combined. Generally, this means compressing or expanding the surface lattice parameters of one of the materials to match the surface lattice parameters of the other material. This can lead to excessive strain if the mismatch between the two materials is great due to a large distortion of one or both of the materials. One method to overcome such strain is near-coincidence-site lattice (NCSL)[34] theory. Rather than combining single surface cells together to form the interface, in NCSL theory, the interface is constructed by combining surfaces composed of multiple cells. For instance, an interface can be formed between the (001) rutile and (100) anatase surfaces that consists of 18.2 Å×22.7 Å and 18.0 Å × 22.3 Å surface cell sizes for rutile and anatase, respectively. This large interface minimizes the misfit between the two surfaces, giving misfit percentage values (a measure of the strain created by putting the two surfaces in a common periodic cell) of 3.47% and −0.92% in the x- and y-directions, respectively.[33] The difficulty, therefore, of modeling such interfaces is predominantly the large system size, requiring robust computational resources.

In order to facilitate computational difficulties, geometries of the interfaces between bulk rutile and anatase were taken from the work of Deskins *et al.*[35] wherein slabs were modeled through molecular dynamics simulations with an empirical forcefield. Full details on these calculations can be found in the previous work of Deskins *et al.* These simulations were performed in the isothermal/isobaric (NPT) ensemble, so that the lattice vectors were relaxed at the given temperature and pressure. These interfaces were then modeled at the DFT level, albeit single-point calculations, not full relaxation. Using empirical forcefields allows for a large sampling of the geometry space in tractable simulation time. The interfaces in this previous work were constructed by bringing together surfaces with thousands of atoms in size together and then subjecting them to an annealing procedure in order to better obtain realistic structures. The interfaces were simulated at 1300 K, and then slowly annealed to low temperature. Such simulations are typically beyond the capabilities of current DFT methods, given the large size of the system. For an interface between the rutile (001) and anatase (100) surfaces, the supercell had 2472 atoms and the total size of the slab was 18.2 Å by 22.7 Å in the x- and y-directions, respectively. The slab was ~60.2 Å in the z direction with a ~20 Å vacuum spacing between slabs. Figure 1 shows the supercell slab model used. An alternative interface that was also used in this work was formed between the rutile (110) and anatase (101) surfaces and had 1136 atoms. There are other interfaces between various surfaces that could have been used, but these contained larger number of atoms,[35] and therefore are more difficult to model.

We also modeled interfaces between rutile and anatase with exposed surfaces, where for instance surface chemistry may occur (see Figure 8). Such a region is essentially a three-phase region with rutile, anatase, and vacuum all adjacent to each other. This structure was not used to calculate band offsets, but to identify the electronic properties of the interfacial region. The structure of this interface was created using a molecular dynamics approach. Interatomic interactions were represented by the Buckingham potential with the parameters

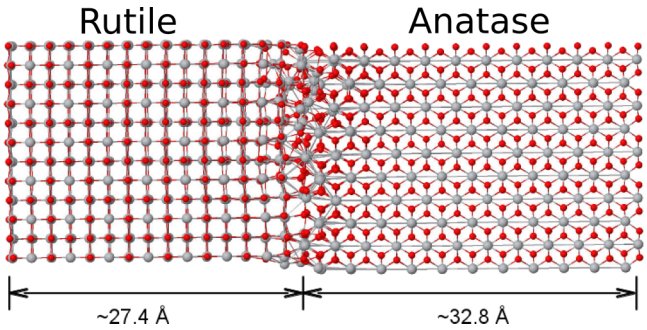

FIG. 1. Slab model of the interface between bulk materials used in the current work formed by bringing together the rutile (001) and anatase (100) surfaces. The thickness of each phase is indicated. The red spheres represent oxygen, the grey spheres represent Ti. The same color scheme is used in the remaining figures. The vacuum region is along the x direction and extends ~20 Å beyond the edges of the rutile and anatase materials.

from the work of Matsui and Akaogi.[36] The calculations were performed with the DL_POLY[37] code. A cutoff distance of 9.0 Å was used for the short-range interactions. We performed all calculations in the NPT ensemble. We started our molecular dynamic simulation at 800 K for 400 ps using a timestep of 0.001 ps. Then, the temperature was lowered in 100 K increments for 200 ps at each temperature until 0 K was reached. Next, we optimized the structure at 0 K for 200 ps. The final structure was simulated at the DFT level. This surface interface had 1056 atoms and the simulation box had dimensions of 14.9 Å by 55.2 Å by 30.0 Å. The vacuum space between surfaces was 20 Å.

Due to the large size of the systems and computational limitations, we only calculated single-point energies and wavefunctions of the slab at the DFT level. Even such single-point calculations were difficult, and typically took several days on a 256-processor cluster. The majority of calculations were performed with code CP2K, which implements the Gaussian and plane waves (GPW) method.[38,39] Valence electrons are described by a double-ζ basis set.[40] Core electrons were described by Goedecker-Teter-Hutter (GTH) pseudopotentials[41] with 12 and 6 valence electrons, respectively, for Ti and O. The gamma point supercell approach was used. Calculations were performed using the Perdew-Burke-Ernzerhof (PBE) exchange correlation functional[42,43] and were all spin-polarized. The auxiliary planewave basis set was expanded up to an energy cutoff of 300 Ry.

A few calculations on the interface were performed with the Vienna *Ab Initio* Simulation Package (VASP) version 5.2[44–47] using three dimensional periodic boundary conditions with a plane wave basis set and a cutoff energy of 400 eV. Projector augmented wave potentials[48,49] are used to describe the core-valence interaction, with 4 and 6 valence electrons and Ti and O, respectively. The PBE exchange-correlation functional[50,51] was used.

One potential problem with DFT simulations is that generalized gradient approximation (GGA) exchange correlation functionals incorrectly describe the band gaps of semiconductors and often do not account for electron localisation, arising from the well known self-interaction error (SIE).[52,53] SIE can lead to incorrect electronic levels (e.g., band gaps) and electronic delocalisation, and to overcome this issue with approximate DFT, we used the so-called +U correction to DFT (DFT + U) on the 3d states of the Ti atoms.[54] DFT + U has been used successfully to model several TiO_2 systems.[55–59] An alternative approach is to use hybrid exchange correlation functionals but such calculations are very time-consuming, often an order of magnitude or more slower than GGA-based DFT. Furthermore, previous work shows that DFT + U and hybrid methods give similar results.[60,61] The little additional computational time of the +U correction justifies its use in the current simulations.

The strength of the U correction may influence the calculated valence band minimum and thus calculated band gaps.[62] The nature of our system makes the selection of a suitable U value difficult due to the presence of two phases. We tested several U values, including assigning different U values to Ti atoms in the two phases. We found that choice of U value did not change our overall conclusions as summarized in Table I, where it was found that the electronic bands of anatase are always lower than those of rutile. Since our calculated offsets appear independent of the U value choice, we chose U values that would reproduce the experimental band gaps for bulk TiO_2 calculations. This results in a U value of 8.4 eV for rutile and 6.3 eV for anatase. For atoms in the interfacial region (defined within 2 Å of interface divide), we assigned an average U value to these Ti atoms (7.4 eV).

We further examined how the U value choice affected our results by calculating the most stable lattice parameters of bulk rutile and anatase as functions of U value. These results are shown in Figures 2(a) and 2(b) and indicate that the lattice parameters are nearly independent of U value choice. These results justify our approach in keeping the simulation cells (i.e., lattice parameters) constant during our work, regardless of U value. We also calculated gap state locations for a (110) rutile surface with a single oxygen vacancy for different U values (Figure 2(c)). We found that below a U value of 4 eV, no electron localization (no gap state) occurred. For U values above 4 eV, the gap state was pushed lower in energy relative to the Fermi level with increasing U value. This highlights the difficulty in choosing a U value since no unambiguous U value choice exists; large U values may give gap states closer to the valence band yet give good band gaps, while smaller U values may give gap states closer to the gap center but too

TABLE I. Electronic bands offsets as calculated using the method in Sec. III B as a function of U parameter for a rutile (001)/anatase (100) interface. Valence band offset (VBO) and conduction band offset (CBO), and band gaps for the anatase-rutile interface using CP2K are given. In all cases, the rutile valence and conduction bands lie higher than the anatase bands.

U (eV)				Band gap (eV)	
Anatase	Rutile	VBO (eV)	CBO (eV)	Anatase	Rutile
0.0	0.0	0.81	0.46	2.11	1.77
4.0	4.0	1.05	0.54	2.84	2.34
8.0	8.0	1.21	0.66	3.47	2.92
10.0	10.0	1.31	0.70	3.89	3.28
6.3	8.4	0.41	0.21	3.20	3.00

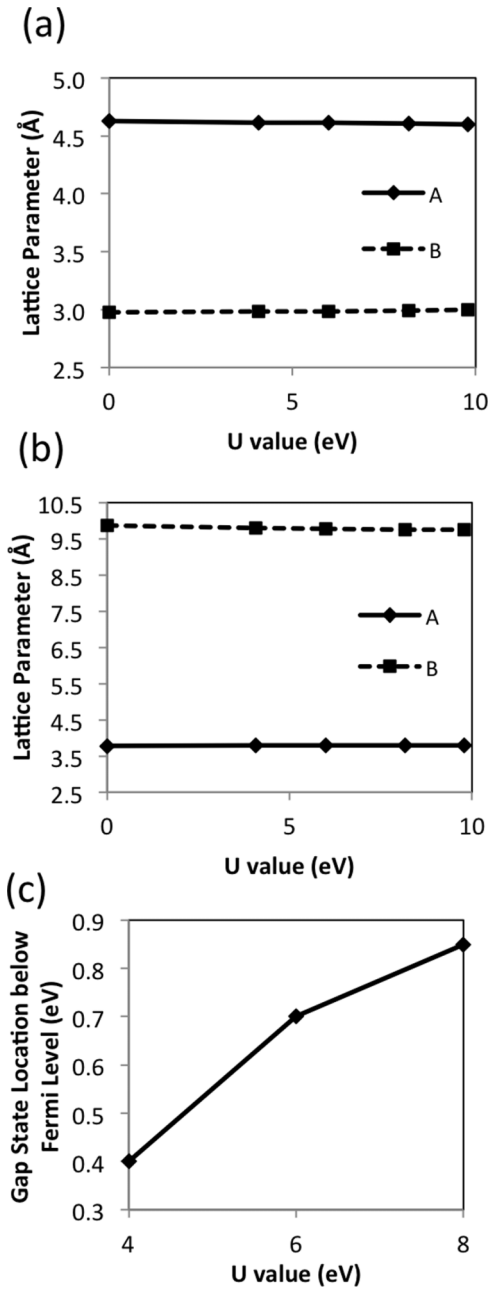

FIG. 2. Further results on the effect of U value choice for TiO_2 systems. (a) Calculated lattice parameters of bulk rutile. (b) Calculated lattice parameters of bulk anatase. (c) Calculated gap state location relative to the Fermi level. A more positive energy value corresponds to a gap state lower in energy relative to the Fermi level.

small band gaps. Nonetheless, we conclude that for sufficiently large U values (>4 eV), appropriate gap states can form in TiO_2 systems, albeit the exact location of such a state may vary. As a final examination of the U value choice, we compare with reported literature values. U values for Ti in the range of 2–8 eV have been reported, as discussed by Nolan *et al.*,[63] for different oxides, oxidation states, and exchange correlation functionals. For instance, Jedidi *et al.*[64] used a U value of 8 eV to model photoexcitation in rutile. A recent paper[65] used an iterative procedure to determine a Hubbard U value of 7.5 eV based on refining the U value choice in combination with the GW approximation. This literature U value is very close to our average U value of 7.4 eV.

For the VASP calculations, we used U = 4.5 eV, in the range of calculations using a similar plane-wave basis set/pseudopotential.[60,66] The choice of 4.5 eV for VASP, while less than the values used by CP2K, gives qualitative agreement with CP2K calculations as discussed further in the paper. The difference in appropriate U values for the two codes can be explained based on differences in the two codes; CP2K uses the Gaussian and plane waves approach, while VASP uses a plane waves basis set. In the end, it must be remembered that the DFT + U method is an arbitrary correction, and that the appropriate U value choice may depend on simulation parameters such as basis set, pseudopotential, and k-point mesh. The appropriate U value choice may also depend on how the +U method is implemented within a certain code. A U value from one set of calculations is not necessarily transferable to another set of calculations, especially if different properties are being studied. Further data, likely from experiment, are needed to clarify what the most appropriate U value choice is for TiO_2 interfaces. We, however, believe our choice of U values to give meaningful results on the nature of the mixed-phase interfaces based on our testing of the U value choice and comparison with literature values.

III. RESULTS AND DISCUSSION

A. Nature of the interface

Our procedure to produce the interface does not simply rely on bringing two surfaces together to form a heterostructure and then allowing optimization (a common approach). Rather, rearrangement and relaxation of the interfacial region is accomplished through the simulated annealing approach discussed in Sec. II. While time-consuming, such an approach gives interfaces that are more likely representative of those present between real TiO_2 nanoparticles. During synthesis and reaction conditions, the interfacial atoms between particles are likely to overcome any energetic barriers for rearrangement and find more stable configurations. A standard optimization procedure is unlikely to find any such configurations. The final relaxed interfacial region exists as a transition between the two phases since rutile is more stable than anatase, and the interface region is disordered (see Figure 1). These interface regions have been observed experimentally and are suggested to be crucial for the anatase-to-rutile phase transition.[67–69] The local surface structure of the two materials, e.g., (001) and (100) is largely removed as surface atoms lose their ordered structure and rearrange to form bonds with the corresponding counter surface.

The interfacial region has a distribution of four-, five-, and six-coordinated Ti atoms. Ti atoms in bulk TiO_2 are six-coordinated. There is no unambiguous way to define coordination, but we assigned coordination numbers based on a simple rule of counting a neighboring atom closer than less than sixty percent of the sum of the van der Waal radii of each pair of atoms (2.0 Å for Ti, 1.3 Å for O), or 1.98 Å. For instance in the rutile (001)/anatase (100) interface (Figure 1), the distribution of coordination on the interfacial Ti atoms was found to be

as follows: 72.2% Ti_{6c}, 22.2% Ti_{5c}, and 5.6% Ti_{4c}, where the subscript designates the coordination. Four-coordinated Ti atoms have been implicated as contributing to increased photoreactivity[70–72] and we discuss their role in future sections of this paper. The distribution of four-coordinated Ti atoms seems to be random for all the interfaces that we studied, that is no discernible trend in position of under-coordinated Ti atoms was found.

We note that recent papers have modeled interfaces between rutile and anatase using density functional theory. A paper by Xia *et al.*[73] addressed the thermal properties of the rutile-anatase interface in order to further clarify the anatase to rutile transition. Kullgren *et al.*[74] calculated the electronic offset between rutile and anatase and found that rutile does indeed have a higher valence and conduction band offsets than anatase. They found that mobile electrons will be accumulated in anatase and holes in rutile. Li *et al.*[75] also studied mixed phase TiO_2 composite slabs using DFT. They concluded that the HOMO and LUMO states are separated in the different phases, which could be the key to improved photoactivity through charge separation. The current paper is unique in that the interfacial region is examined in detail including the electronic structure of this region, which is crucial for these mixed-phase catalysts. None of the previous papers have identified interfacial electronic trapping sites (discussed further below) that are predicted to exist experimentally. The current work also utilizes a large bulk interface, for instance of the size 18.2 Å by 22.7 Å, containing 2472 atoms. The problem with smaller interfaces is that they introduce excess strain as lattices are compressed or stretched to fit together. Relaxation may also be hindered if the interface is too small since the atoms do not have the configurational freedom to fully move and reach more stable configurations. The limited number of unique atoms and periodic boundary conditions may prevent the realization of realistically optimized structures. Thus, bigger interfaces are likely to give results more comparable to experimental results.

B. Electronic offsets between the phases

The key to aligning energy levels of two materials is to find a common reference level. Such an absolute reference can only be present when the energies in the bulk semiconductor can be referenced to the vacuum level or some other common level. Since typical bulk calculations are carried out for an infinite crystal, no such reference is available; the calculated energy bands are referred to an average electrostatic potential within the solid, which is only defined with respect to an arbitrary constant.[76,77] In order to align the energy levels of the two phases, we used the macroscopic average of the electrostatic potential in the supercell as proposed by Baldereschi *et al.*[29] and Fall *et al.*[28] This method filters the microscopic periodic oscillations and gives the macroscopic electrostatic properties.

The valence band offset, ΔE_{VBO}, is defined as the difference between the valence band maximum (VBM) of the two phases, and was calculated using the following expression:

$$\Delta E_{VBO} = \Delta E_V + \Delta V, \tag{1}$$

where ΔE_V is the difference between the two bulk band edges as calculated by the DFT program. In this case, the eigenvalues are measured with respect to the average of the electrostatic potential of each individual bulk material. The second term ΔV is the difference in the bulk electrostatic potential as calculated through the electronic distribution and charge on the ion cores. This term accounts for the different reference levels of the two materials and also may contain interfacial effects. ΔV was calculated as follows.

To compute the electrostatic potential along the z-direction of the interfacial slab, electrostatic data generated by CP2K were processed in order to compute the planar electrostatic potential average $\overline{V}$ with the following expression:

$$\overline{V}(z) = S^{-1} \int_S V(\vec{r}) dx dy. \tag{2}$$

In Eq. (2), S is the area of the plane perpendicular to the z direction, and x, y are contained in that plane. After computing the planar electrostatic average, $\overline{V}$, it was required to determine the macroscopic average of the electrostatic potential in the slab. To achieve this goal, we used a local averaging scheme. This was performed taking an arithmetic average of the nearest neighbors of the point. The result of such procedure is shown in Figure 3. Once the electrostatic potential average was computed, the difference was taken from the electrostatic values in the bulk-like region of each phase, where the potential was virtually constant (~15 Å and ~50 Å in Figure 3) to give ΔV. We also performed separate bulk calculations for each phase and computed the difference between the energy of HOMO (valence band maximum) and the average electrostatic potential (which is aligned to the interface average electrostatic potential). In this manner, we have the energy of the valence band maxima referenced to the average potential for each phase.

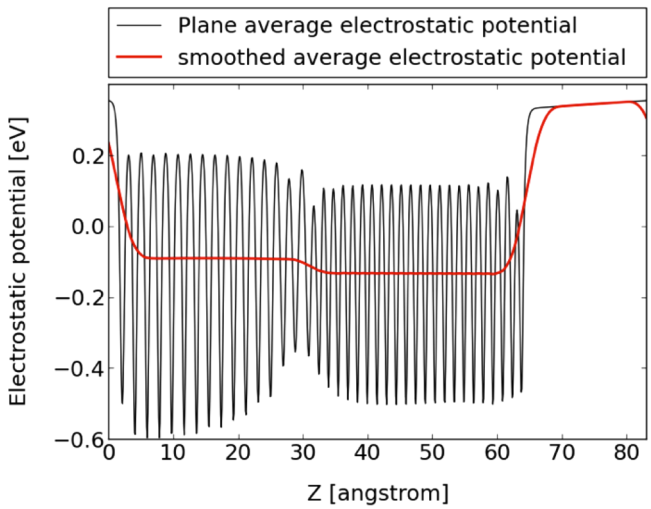

FIG. 3. Average electrostatic potential variation along the z axis of the mixed phase rutile (001)/anatase (100) slab using CP2K and U values of 8.4/6.3 eV for rutile/anatase. The black line represents the average potential in planes perpendicular to the z axis ($\overline{V}$) and the red line represents a smoothed average. The difference between the two smoothed averages in the middle of the slabs gives ΔV.

A sample result showing the calculated bulk offsets is shown in Figure 4. We calculated rutile to have a higher conduction band offset than anatase by 0.21 eV, and a higher valence band offset of 0.41 eV for U values of 8.4/6.3 eV, respectively, for rutile/anatase. This alignment would produce an accumulation of bulk migrating electrons in the anatase phase accompanied by hole accumulation in the rutile phase, suggesting that charge separation does indeed occur for a TiO_2 heterostructure. Table I summarizes results using various U values, and we found that the direction of offset (rutile higher than anatase) does not change based on the U value choice, only the magnitude of the offset. Thus, the DFT + U results are all consistent with the picture in Figure 4 for electronic band offsets. The results for the other studied interface, an interface between the rutile (110) and anatase (101) surfaces, presented the same trend with a CBO of 0.18 eV.

In contrast, previous experimental work[15] argued that the anatase CB was higher than the CB of rutile. However, this previous work did not actually measure the offset between the two materials, but inferred the offset based on other measured properties, such as x-ray diffraction data. Other experimental work[20] used x-ray photoelectron spectroscopy (XPS) to show an alignment with rutile having higher offsets than anatase.

Theoretical work generally agrees with our current work. The exception appears to be the work of Kang *et al.*[78] who computed through DFT a different band alignment than our work, and suggested that anatase has a higher VB and CB. They used the LDA (local density approximation) exchange correlation functional (no U correction) and modeled particles, rather than bulk TiO_2, which could explain the disagreement with our work. On the other hand, other recent theoretical results agree with our conclusions. Using the branching point energy or charge neutrality level as a common reference,[27,79] Deák *et al.*[19] found the rutile CB to be higher than the anatase CB by 0.3 to 0.4 eV. This work is based on a more crude alignment procedure (no common cell between rutile and anatase was modeled) but the agreement with our work is encouraging. Later work by this group[74] also found the rutile CB to be higher than the anatase CB by modeling rutile/anatase interfaces, utilizing an alignment scheme similar to the current work. Our values are also reasonably consistent with those from embedded cluster hybrid DFT results.[20] In previous DFT work, Deskins and Dupuis[80] also predicted the same trends in phase preference of the charges based on the thermodynamics of electron/hole transfer to the two phases. Furthermore, Li *et al.*[81] developed a theoretical model where the electrons in TiO_2 have small polaron character in the rutile phase. Their model also predicted that the rutile CB lies higher than the anatase CB. We conclude that the alignment scheme from theory is fairly consistent, but that more work may be needed to reconcile experimental observations and theoretical predictions.

In order to further examine the effect of the interface, we performed an analysis of the projected density of states (PDOS) for the slab, with the density of states calculated for different regions of the interface model. Figure 5 shows the PDOS around the VB and CB of the slab. The PDOS for each atom type was found, then the PDOS were added together to get the DOS of the rutile, anatase, and interface regions. The bulk rutile and anatase PDOS were taken ~10 Å away the interface, or in the middle of the anatase and rutile regions of the slab (representative of the bulk phases), while the interfacial PDOS included atoms within 2 Å of the interfacial divider. The results from the PDOS agree with our previous offset results (Figure 4) in that the bulk CB and VB of rutile are both higher than that of anatase. We also observed an interfacial gap state (discussed in Sec. III C) just below 0 eV.

Our results discussed so far have been performed with CP2K utilizing the Gaussian and plane wave method.[38,39] We have also performed density of states analysis using VASP on the the rutile (001)/anatase (100) interface model, with U = 4.5 eV. VASP utilizes a plane wave basis set, so provides another simulation method to evaluate the electronic properties of mixed-phase slab. We obtained localized density of states and selected atoms in bulk regions of the slab for analysis. These bulk regions were defined as in between the exposed surface and interface regions and have bulk-like geometries. Similar to the results above, we found the rutile valence states to lie higher in energy than the corresponding anatase states (Figure 6), confirming our offset predictions with two different DFT methods.

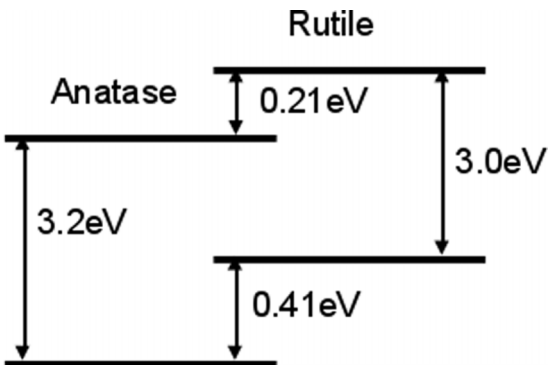

FIG. 4. Schematic representation of the band alignment between rutile and anatase as calculated by DFT + U (U = 8.4/6.3 eV for rutile/anatase) and the rutile (001)/anatase (100) interface.

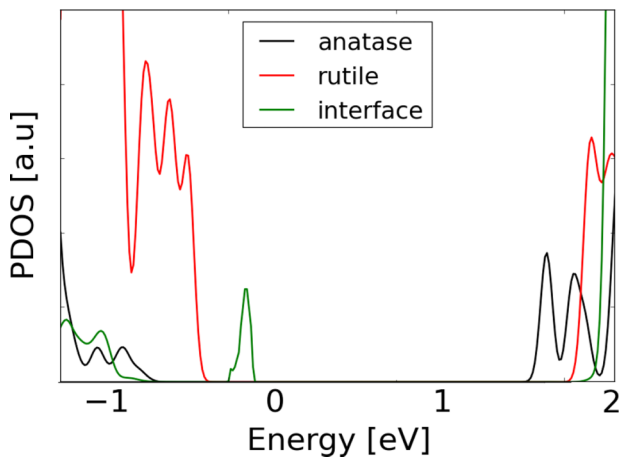

FIG. 5. PDOS plot for the anatase phase, rutile phase, and the interface region using U = 8.4/6.3 eV for the rutile (001)/anatase (100) interface using the CP2K code. 0 eV corresponds to the Fermi level.

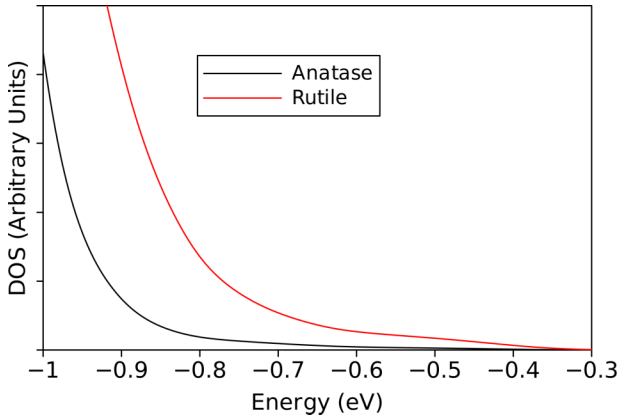

FIG. 6. Localized electronic density of states plot for different bulk regions of a rutile (001)/anatase (100) interface. Results were calculated using the VASP program. Zero corresponds to the Fermi level. U = 4.5 eV was used for these calculations.

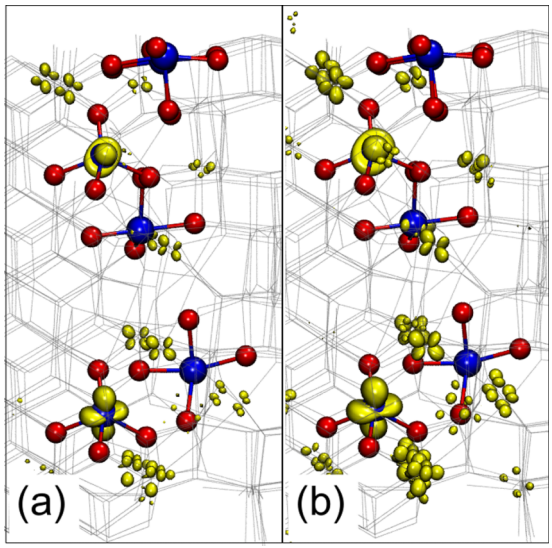

FIG. 7. (a) Electron spin density plot (isovalue = 0.017e/Å^3) of electrons localized in the 3d orbitals of four coordinated Ti atoms in the interfacial region for a neutral slab. The results are from a rutile (001)/anatase (100) interface with U = 8.4/6.3 eV for rutile/anatase. (b) An electron spin density plot (isovalue = 0.03e/Å^3) for a slab having a net −1 charge. No +U correction was applied to these calculations. The blue spheres represent four coordinated Ti atoms while red spheres are their nearby O atoms. The yellow contours represent the spin up density.

C. Charge trapping at four-coordinated Ti

As mentioned above, a gap state is observed in the PDOS, as shown in Figure 5, which represents the localization of electrons within the interfacial region. In our model slab, the interfacial region has a disordered structure due to the transition from one phase to the other, and the Ti atoms have a variety of coordination numbers.[35] We identified five Ti atoms that were four-coordinated (Ti_{4c}) in the rutile (001)/anatase (100) interface and several electrons localized at some of these sites, as shown in Figure 7. Large electron spin density is found in d orbitals on Ti_{4c} atoms. The gap state observed in Figure 5 corresponds to the localization of electrons at these Ti_{4c} sites. The location of the gap state is U value dependent and smaller U values may lead to gap states further above the valence band. There are some electrons localized on other interfacial Ti atoms besides the two Ti_{4c} atoms, but there is much less electron density on these atoms. We did not observe unpaired electrons away from the interface (bulk rutile and anatase) region of the slab.

Not all Ti_{4c} atoms in the interface had localized excess electrons and, in fact, we observed no localized electrons for the rutile (110)/anatase (101) interface which only had two Ti_{4c} in the interface. These results show that merely the presence of Ti_{4c} does not guarantee electron localization and formation of gap states; such processes are structure dependent. The greater number of Ti_{4c} in the rutile (001)/anatase (100) interface, however, leads to a greater chance of electron localization which is why electron localization is observed for this interface while no localization occurs for the rutile (110)/anatase (101) interface.

One issue arising from these calculations is the nature of the hole states. Since unpaired electrons localized at specific Ti_{4c} sites, forming Ti^{3+} cations, hole states on O atoms must also have formed in the slab due to electron deficiency. We found these hole states to be delocalized across several O atoms rather than confined to specific atoms. This delocalization of the holes could possibly be mitigated by applying DFT + U to the O orbitals, but should not change the conclusions on electron localization. In order to further remove the issue of hole states and address the stability of photoexcited electrons at or near the interfacial region, we simulated a slab that had a net charge of −1, in contrast to previous results thus far which involved neutral slabs. A similar approach was used to model polaron formation in bulk TiO_2.[82] Electron spin density plots of the interfacial region using a charged slab are shown in Figure 7(b). In agreement with our previous results on neutral slabs, excess electronic charge occurs at several Ti_{4c} sites. In fact, the extra electron even localizes at Ti_{4c} sites even when no U correction is applied (U = 0 eV or standard GGA-based DFT) indicating the strong tendency of electrons to localize at Ti_{4c} sites and become trapped. A Ti^{4+} atom in bulk TiO_2 is surrounded by six O^{2-} atoms in a stable octahedral environment. Ti_{4c} atoms are deficient in coordination, and therefore deficient in surrounding negative charge and filled bonding. Apparently, this deficiency leads to a destabilization such that addition of an excess electron stabilizes the Ti_{4c}. Such behavior is also seen with surface atoms which have unsaturated bonds, where electron trapping may occur.[83] Previous DFT results have shown that Ti_{4c} can exist on nanoparticle surfaces and can act as sites to trap electrons.[71] The importance of undercoordinated Ti atoms as electron traps has also been discussed from experiments.[9,70]

Undercoordinated Ti has been shown by modeling results to be very reactive for catalysis.[84] At the interface between anatase particles, undercoordinated Ti also have been shown to form trapping states[71] (a similar finding to our current work except that we considered both rutile and anatase phases). Our results thus show that excited electrons could migrate to the interfacial region and become trapped at Ti_{4c} sites. Generally, trapping sites are proposed to increase hole/electron recombination, but it is still unclear whether these interfacial sites have an inhibitory or beneficial effect on photocatalysis. These unpaired electrons may potentially be available to participate in chemical reactions at exposed areas of the interface, and

could be photocatalytic "hot spots."[70] These Ti_{4c} sites have been shown experimentally[9] to exist in the transition region between rutile and anatase, and have been postulated as increasing the reactivity of mixed-phase TiO_2. We note that distorted tetrahedral shapes were also observed for four-coordinated Ti on anatase particle surfaces.[71] Our results do indeed confirm the special nature of the interface and the existence of Ti_{4c}, as well as their trapping nature. Synthesis of TiO_2 materials with increased interfacial Ti_{4c} atoms may be an avenue to develop more active photocatalysts and more experimental and theoretical work is needed to further clarify the nature of undercoordinated atoms for photocatalysis.

D. Exposed surfaces of mixed phase TiO_2

Our studies so far on mixed phase surfaces have been focused by modeling bulk interfaces. In this section, we discuss results on modeling a surface of a mixed phase anatase/rutile material, or a three-phase system (anatase, rutile, and vacuum). Such interfaces would be present for instance at the intersection of two nanoparticles (rutile and anatase). This approach requires a large supercell in order to accommodate the two pure phases plus the interfacial region. The amorphous character of the interface between the phases adds an additional complication to the molecular model of the surfaces.

We modeled a slab with two different distinct interfaces (due to the periodic boundary conditions). This slab had two different phases brought together and two different vacuum-exposed surfaces. The vacuum-exposed surfaces are the (110) surface for rutile and (101) for anatase, which are shown in Fig. 8. Those are the most stable surfaces for each phase. The slab has two interfaces due to the present periodic boundary conditions in the x and y directions. There is a vacuum space in the z-direction of ~20 Å between slabs. This geometry was built using molecular dynamics and the cooling approach described in Sec. II. This structure represents a surface environment where a molecule may potentially adsorb in the interfacial region and react.

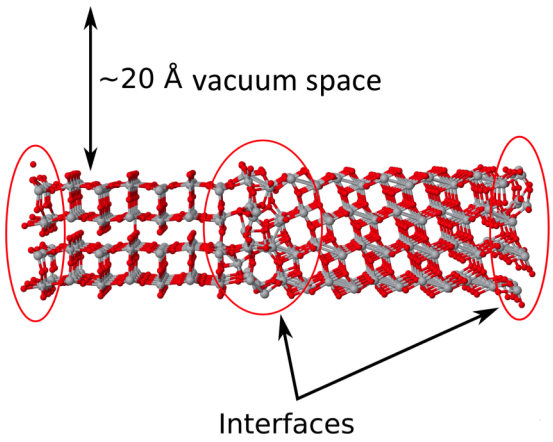

FIG. 8. Slab model of the mixed phase exposed surface. Two interfaces exist for this slab and the anatase and rutile surfaces are both exposed to vacuum, including the interfacial region. The interface regions on the far left and far right are the same interfaces due to the periodic boundary conditions.

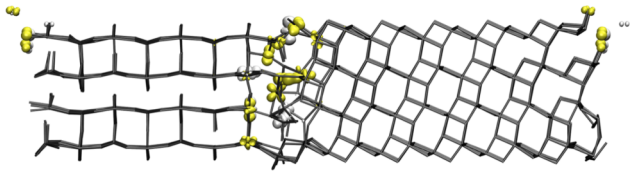

FIG. 9. Spin up and down density plot showing the whole slab (isovalue = 0.017e/Å^3). The yellow contours represent the spin up density and the white surfaces represent the spin down density. The grey lines represent the bonds between atoms.

Localization of charge was observed in this system in the interface. This can be visualized with a spin density plot, as shown in Fig. 9. From this figure, it is clear that the unpaired electrons are more stable within the interfacial region than in the pure phases alone. Electrons seem to be trapped in this disordered region. These results agree with our previous results using a bulk interface, and we now confirm the trapping nature of a surface interface. Therefore, the interfacial region is potentially more reactive, since localized electrons could be transferred to adsorbates on the surface near the interfaces.

To further clarify the interfacial region, Fig. 10 shows only the Ti atoms in the interfacial region and the spin density isosurfaces for the electrons with spin up and down. The majority of the atoms in this interface model are five- and four-coordinated, the purple and green spheres in Fig. 10, but even six and three-coordinated atoms are found. The electrons can be seen localized mostly on the five and four coordinated Ti atoms. There are also unpaired electrons in one of the two three coordinated Ti Atom and in one of the two six coordinated Ti atoms in this region. In general, the distortion of the lattice seems to favor the stability of unpaired electrons on undercoordinated Ti atoms. The results of a slab with exposed surfaces give very similar results to bulk interfaces, which confirm the electron trapping character of the interfacial region.

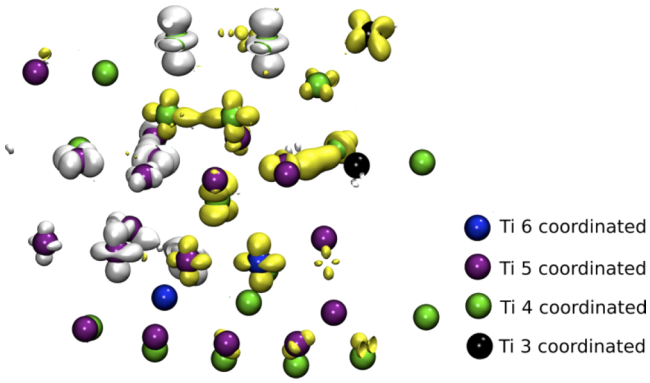

FIG. 10. Electron spin density plot (isovalue = 0.017e/Å^3) of the interfacial region for a slab with vacuum-exposed surfaces. The results are from a rutile (001)/anatase (100) interface with U = 8.4/6.3 eV for rutile/anatase. The blue spheres represent six coordinated Ti atoms, the purple spheres represent five coordinated Ti atoms, the green spheres represent four coordinated Ti atoms, and the black spheres represent three coordinated Ti atoms. The yellow contours represent the spin up density and the white surfaces represent the spin down density.

IV. CONCLUSIONS

We have simulated the interface between the anatase and rutile phases of TiO_2 using DFT + U in order to better characterize the nature of mixed-phase TiO_2 photocatalysts. We modeled realistic structures that contained thousands of atoms, rather than smaller, possibly irrelevant interfaces. Our results show that the rutile conduction and valence bands are higher than the anatase bands. This has important implications for TiO_2 photocatalysis, indicating the preferred direction of electron/hole flow (electrons to anatase, holes to rutile). Such preferred migration could lower the electron/hole recombination rate, which would increase photo-reactivity. Our results are also particularly novel, in that, we show how electron trapping can occur in the interfacial region in bulk and exposed slabs at undercoordinated Ti sites. Such sites have been experimentally predicted, but theoretical work now confirms their existence. Trapped electrons produce a gap state, which may influence photoexcitation, and these trapping sites may also strongly influence electron/hole recombination and/or reactivity. Such trapping may be strong and in fact a charged slab (−1 net charge) exhibited electron localization with no +U correction. Finally, we acknowledge that we have modeled interfaces formed from stoichiometric surfaces. We cannot exclude the possibility that defects (such as O vacancies or Ti interstitials) may affect the electronic properties of mixed-phase interfaces, and future work may examine interfaces with such structures.

ACKNOWLEDGMENTS

Computational resources were provided by the Molecular Science Computing Facility at the Environmental Molecular Science Laboratory of Pacific Northwest National Laboratory. Battelle operates Pacific Northwest National Laboratory for the U.S. Department of Energy. We also thank Sia Najafi at WPI for his support in using WPI computer resources. M.N. acknowledges support from Science Foundation Ireland through the Starting Investigator Research Grant Program, project "EMOIN" Grant No. SFI 09/SIRG/I1620. We also acknowledge computing resources provided by SFI to the Tyndall National Institute and by the SFI and Higher Education Authority Funded Irish Centre for High End Computing. Support from the European Commission for access through the FP7 Research Infrastructures Project PRACE-RI is gratefully acknowledged. We acknowledge support from the European Union through the COST Action CM1104 "Reducible Oxide Chemistry, Structure, and Functions."

[1]U. Diebold, Surf. Sci. Rep. **48**, 53 (2003).
[2]T. Ohno, K. Sarukawa, K. Tokieda, and M. Matsumura, J. Catal. **203**, 82 (2001).
[3]M. Yan, F. Chen, J. Zhang, and M. Anpo, J. Phys. Chem. B **109**, 8673 (2005).
[4]D. Hurum, A. Agrios, K. Gray, T. Rajh, and M. Thurnauer, J. Phys. Chem. B **107**, 4545 (2003).
[5]W. Li, C. Liu, Y. Zhou, Y. Bai, X. Feng, Z. Yang, L. Lu, X. Lu, and K. Chan, J. Phys. Chem. C **112**, 20539 (2008).
[6]G. Li, S. Ciston, Z. Saponjic, L. Chen, N. Dimitrijevic, T. Rajh, and K. Gray, J. Catal. **253**, 105 (2008).
[7]L. Shi and D. Weng, J. Environ. Sci. **20**, 1263 (2008).
[8]K. Connelly, A. Wahab, and H. Idriss, Mater. Renewable Sustainable Energy **1**, 3 (2012).
[9]G. Li, N. Dimitrijevic, L. Chen, J. Nichols, T. Rajh, and K. Gray, J. Am. Chem. Soc. **130**, 5402 (2008).
[10]A. Linsebigler, G. Lu, and J. Yates, Chem. Rev. **95**, 735 (1995).
[11]W.-J. Yin, H. Tang, S.-H. Wei, M. M. Al-Jassim, J. Turner, and Y. Yan, Phys. Rev. B **82**, 45106 (2010).
[12]M. Ni, M. K. H. Leung, D. Y. C. Leung, and K. Sumathy, Renewable Sustainable Energy Rev. **11**, 401 (2007).
[13]W. Choi, A. Termin, and M. R. Hoffmann, J. Phys. Chem. **98**, 13669 (1994).
[14]A. Sclafani and J. M. Herrmann, J. Phys. Chem. **100**, 13655 (1996).
[15]T. Kawahara, Y. Konishi, H. Tada, N. Tohge, J. Nishii, and S. Ito, Angew. Chem. **114**, 2935 (2002).
[16]M. Henderson, Surf. Sci. Rep. **66**, 185 (2011).
[17]G. Li, L. Chen, M. E. Graham, and K. A. Gray, J. Mol. Catal. A: Chem. **275**, 30 (2007).
[18]L. Kavan, M. Grätzel, S. E. Gilbert, C. Klemenz, and H. J. Scheel, J. Am. Chem. Soc. **118**, 6716 (1996).
[19]P. Deák, B. Aradi, and T. Frauenheim, J. Phys. Chem. C **115**, 3443 (2011).
[20]D. O. Scanlon, C. W. Dunnill, J. Buckeridge, S. A. Shevlin, A. J. Logsdail, S. M. Woodley, C. R. A. Catlow, M. J. Powell, R. G. Palgrave, I. P. Parkin, G. W. Watson, T. W. Keal, P. Sherwood, A. Walsh, and A. A. Sokol, Nat. Mater. **12**, 798 (2013).
[21]V. Pfeifer, P. Erhart, S. Li, K. Rachut, J. Morasch, J. Brötz, P. Reckers, T. Mayer, S. Rühle, A. Zaban, I. M. Seró, J. Bisquert, W. Jaegermann, and A. Klein, J. Phys. Chem. Lett. **4**, 4182 (2013).
[22]Y. Kho, A. Iwase, and W. Teoh, J. Phys. Chem. C **2**, 2821 (2010).
[23]K. Komaguchi, H. Nakano, A. Araki, and Y. Harima, Chem. Phys. Lett. **428**, 338 (2006).
[24]J. Zhang, Q. Xu, Z. Feng, M. Li, and C. Li, Angew. Chem., Int. Ed. Engl. **47**, 1766 (2008).
[25]S. Leytner and J. T. Hupp, Chem. Phys. Lett. **330**, 231 (2000).
[26]D. C. Hurum, A. G. Agrios, S. E. Crist, K. A. Gray, T. Rajh, and M. C. Thurnauer, J. Electron Spectrosc. Relat. Phenom. **150**, 155 (2006).
[27]J. Tersoff, Phy. Rev. B **30**, 4874 (1984).
[28]C. J. Fall, N. Binggeli, and A. Baldereschi, J. Phys.: Condens. Matter **11**, 2689 (1999).
[29]A. Baldereschi, S. Baroni, and R. Resta, Phys. Rev. Lett. **61**, 734 (1988).
[30]L. Colombo, R. Resta, and S. Baroni, Phys. Rev. B **44**, 5572 (1991).
[31]H.-P. Komsa, E. Arola, E. Larkins, and T. T. Rantala, J. Phys.: Condens. Matter **20**, 315004 (2008).
[32]B. Hoffling, A. Schleife, F. Fuchs, C. Rodl, and F. Bechstedt, Appl. Phys. Lett. **97**, 032113 (2010).
[33]P. W. Peacock and J. Robertson, Phys. Rev. Lett. **92**, 057601 (2004).
[34]T. Sayle, C. Catlow, D. Sayle, S. Parker, and J. Harding, Philos. Mag. A **68**, 565 (1993).
[35]N. A. Deskins, S. Kerisit, K. M. Rosso, and M. Dupuis, J. Phys. Chem. C **111**, 9290 (2007).
[36]M. Matsui and M. Akaogi, Mol. Simul. **6**, 239 (1991).
[37]I. T. Todorov, W. Smith, K. Trachenko, and M. T. Dove, Journal of Materials Chemistry **16**, 1911 (2006).
[38]J. VandeVondele, M. Krack, F. Mohamed, M. Parrinello, T. Chassaing, and J. Hutter, Comput. Phys. Commun. **167**, 103 (2005).
[39]G. Lippert, J. Hutter, and M. Parrinello, Theor. Chem. Acc. **103**, 124 (1999).
[40]J. VandeVondele and J. Hutter, J. Chem. Phys. **127**, 114105 (2007).
[41]S. Goedecker, M. Teter, and J. Hutter, Phys. Rev. B **54**, 1703 (1996).
[42]C. Hartwigsen, S. Goedecker, and J. Hutter, Phys. Rev. B **58**, 3641 (1998).
[43]M. Krack, Theor. Chem. Acc. **114**, 145 (2005).
[44]G. Kresse and J. Hafner, Phys. Rev. B **47**, 558 (1993).
[45]G. Kresse and J. Hafner, Phys. Rev. B **49**, 14251 (1994).
[46]G. Kresse and J. Furthmüller, Comput. Mater. Sci. **6**, 15 (1996).
[47]G. Kresse and J. Furthmüller, Phys. Rev. B **54**, 11169 (1996).
[48]P. E. Blöchl, Phys. Rev. B **50**, 17953 (1994).
[49]G. Kresse and D. Joubert, Phys. Rev. B **59**, 1758 (1999).
[50]J. P. Perdew, K. Burke, and M. Ernzerhof, Phys. Rev. Lett. **77**, 3865 (1996).
[51]J. P. Perdew, K. Burke, and M. Ernzerhof, Phys. Rev. Lett. **78**, 1396 (1997).
[52]M. V. Ganduglia-Pirovano, A. Hofmann, and J. Sauer, Surf. Sci. Rep. **62**, 219 (2007).
[53]G. Pacchioni, J. Chem. Phys. **128**, 182505 (2008).
[54]S. L. Dudarev, G. A. Botton, S. Y. Savrasov, C. J. Humphreys, and A. P. Sutton, Phys. Rev. B **57**, 1505 (1998).
[55]S. Chrétien and H. Metiu, J. Phys. Chem. C **115**, 4696 (2011).
[56]M. F. Camellone, P. M. Kowalski, and D. Marx, Phys. Rev. B **84**, 1 (2011).
[57]J. Stausholm-Møller, H. H. Kristoffersen, B. Hinnemann, G. K. H. Madsen, and B. Hammer, J. Chem. Phys. **133**, 144708 (2010).
[58]P. M. Kowalski, M. F. Camellone, N. N. Nair, B. Meyer, and D. Marx, Phys. Rev. Lett. **105**, 146405 (2010).

[59]B. J. Morgan and G. W. Watson, Surf. Sci. **601**, 5034 (2007).
[60]T. Shibuya, K. Yasuoka, S. Mirbt, and B. Sanyal, J. Phys.: Condens. Matter **24**, 435504 (2012).
[61]E. Finazzi, C. Di Valentin, G. Pacchioni, and A. Selloni, J. Chem. Phys. **129**, 154113 (2008).
[62]M. C. Toroker, D. K. Kanan, N. Alidoust, L. Y. Isseroff, P. Liao, and E. A Carter, Phys. Chem. Chem. Phys. **13**, 16644 (2011).
[63]M. Nolan, S. D. Elliott, J. S. Mulley, R. A. Bennett, M. Basham, and P. Mulheran, Phys. Rev. B **77**, 235424 (2008).
[64]A. Jedidi, A. Markovits, C. Minot, S. Bouzriba, and M. Abderraba, Langmuir **26**, 16232 (2010).
[65]C. E. Patrick and F. Giustino, J. Phys. Condens.: Matter **24**, 202201 (2012).
[66]B. J. Morgan and G. W. Watson, J. Phys. Chem. C **114**, 2321 (2010).
[67]R. L. Penn and J. F. Banfield, American Mineralogist **84**, 871 (1999); available at: http://www.minsocam.org/msa/ammin/toc/1999/MJ99.html.
[68]G. H. Lee and J.-M. Zuo, J. Am. Ceram. Soc. **87**, 473 (2004).
[69]H. Zhang and J. F. Banfield, J. Phys. Chem. B **104**, 3481 (2000).
[70]G. Li and K. A. Gray, Chem. Phys. **339**, 173 (2007).
[71]F. Nunzi, E. Mosconi, L. Storchi, E. Ronca, A. Selloni, M. Gratzel, and F. De Angelis, Energy Environ. Sci. **6**, 1221 (2013).
[72]J. Zhang, Y. Hu, M. Matsuoka, H. Yamashita, M. Minagawa, H. Hidaka, and M. Anpo, J. Phys. Chem. B **105**, 8395 (2001).
[73]T. Xia, N. Li, Y. Zhang, M. B. Kruger, J. Murowchick, A. Selloni, and X. Chen, ACS Appl. Mater. Interfaces **5**, 9883 (2013).
[74]J. Kullgren, H. A. Huy, B. Aradi, T. Frauenheim, and P. Deák, Phys. Status Solidi RRL **8**, 566 (2014).
[75]W.-K. Li, P. Hu, G. Lu, and X.-Q. Gong, J. Mol. Model. **20**, 2215 (2014).
[76]C. Mitra, B. Lange, C. Freysoldt, and J. Neugebauer, Phys. Rev. B **84**, 193304 (2011).
[77]C. G. Van de Walle, Phys. Rev. B **39**, 1871 (1989).
[78]J. Kang, F. Wu, S.-S. Li, J.-B. Xia, and J. Li, J. Phys. Chem. C **116**, 20765 (2012).
[79]C. G. Van de Walle and J. Neugebauer, Nature **423**, 626 (2003).
[80]N. A. Deskins and M. Dupuis, J. Phys. Chem. C **113**, 346 (2009).
[81]G.-L. Li, W.-X. Li, and C. Li, Phys. Rev. B **82**, 235109 (2010).
[82]N. A. Deskins and M. Dupuis, Phys. Rev. B **75**, 195212 (2007).
[83]A. Cordones and S. Leone, Chem. Soc. Rev. **42**, 3209 (2013).
[84]M. Posternak, A. Baldereschi, and B. Delley, J. Phys. Chem. C **113**, 15862 (2009).